



# Formation energies of silicon self-interstitials using periodic coupled cluster theory

Faruk Salihbegović , Alejandro Gallo, and Andreas Grüneis 

*Institute for Theoretical Physics, Vienna University of Technology, A-1040 Vienna, Austria, EU*



(Received 21 June 2023; accepted 22 August 2023; published 12 September 2023)

We present a study of the self-interstitial point defect formation energies in silicon using a range of quantum chemical theories, including the coupled cluster (CC) method within a periodic supercell approach. We study the formation energies of the X, T, H, and C3V self-interstitials and the vacancy V. Our results are compared to findings obtained using different *ab initio* methods published in the literature and partly to experimental data. In order to achieve computational results that are converged with respect to the system size and basis set, we employ the recently proposed finite-size error corrections and basis set incompleteness error corrections. Our coupled cluster with singles, doubles, and perturbative triples [CCSD(T)] calculations yield an order of stability of the X, H, and T self-interstitials, which agrees both with quantum Monte Carlo results and with predictions obtained using the random-phase approximation as well as using screened hybrid functionals. Compared to quantum Monte Carlo results with backflow corrections, the CCSD(T) formation energies of X and H are only slightly larger by about 100 meV. However, in the case of the T self-interstitial, we find significant disagreement with all other theoretical predictions. Compared to quantum Monte Carlo calculations, CCSD(T) overestimates the formation energy of the T self-interstitial by 1.2 eV. Although this can partly be attributed to strong correlation effects, more accurate electronic structure theories are needed to understand these findings.

DOI: [10.1103/PhysRevB.108.115125](https://doi.org/10.1103/PhysRevB.108.115125)

## I. INTRODUCTION

After more than 60 years of sophisticated silicon device production, one might think that all the details of this material are fully understood, especially knowing that the manufacturing of today's nanometer-sized transistors requires near-atomic accuracy. However, as a direct result of this miniaturization, the accidental creation of a single trapping center can be large enough to alter the electronic properties of the sample, making this issue the most feared phenomenon in the industry [1].

To better understand the influence of single isolated vacancies and interstitials, they have to be produced experimentally. This can be achieved with 1–3 MeV electron irradiation performed at cryogenic temperatures. The identification of these centers is possible through characterization techniques like electron paramagnetic spectroscopy, which is capable of targeting the atomic distortion triggered by the form of the localized electronic density [2,3]. Infrared optical absorption and deep-level transient spectroscopy can also be used to identify center-induced states within the semiconductor gap [4–6]. The availability of experimental data motivated the development of simple theoretical models geared towards quantitatively reproducing the basic features of these defects. Furthermore, the rapid growth in computational resources made it possible to perform *ab initio* calculations to model and understand their properties thoroughly on an atomistic level.

Point defects, such as vacancies, interstitials, and anti-site defects, are the only thermodynamically stable defects at finite temperatures [7]. The presence of point defects often controls the kinetics of the material and can therefore fundamentally alter its electronic, optical, and mechanical properties.

This makes the understanding of point defects technologically important for a wide range of applications such as doping of semiconductors [8–11], production of quantum devices [12,13], and controlling the transition temperature of shape memory alloys [14].

Of all materials, silicon is one of the most important for industrial use and plays a crucial role in a wide variety of devices, e.g., advanced electronic devices, power devices, solar cells, and microelectronic systems. In all these applications, Czochralski and floating zone silicon single crystals are used (except in some solar cells) [15]. The diffusion characteristics and thermodynamics of silicon self-interstitials and vacancies dominate the doping and annealing processes for electronics applications [9,10]. However, the understanding of self-diffusion in silicon remains incomplete despite decades of research [8,11,12,16–34]. Questions regarding the role of the self-interstitials and the vacancy in the self-diffusion remain. One of the remaining questions, which needs to be addressed using quantum mechanical methods, is the formation energy of the silicon self-interstitials and vacancy. The most widely used method in this regard is density functional theory (DFT), which replaces the complicated many-body electron interactions with quasiparticles interacting via an exchange and correlation functional. Exchange and correlation functionals based on the local density approximation (LDA), general gradient approximation, and hybrid functionals predict formation energies in the range of 2–4.5 eV [21]. Green's function based methods, such as the *GW* approximation, are expected to yield more accurate results and predict formation energies of about 4.5 eV [18]. A low-scaling implementation of the random-phase approximation reported formation energies on a similar scale [35]. Quantum Monte Carlo (QMC) provides another computationally more expensive alternative to DFT

and is among the most accurate electronic structure methods available. Several groups have calculated the formation energies using QMC [34,36]. In this work, we focus only on the former [34] because it employs a Slater-Jastrow-backflow wave function, which changes the formation energies substantially.

The coupled cluster (CC) method is a systematically improvable many-electron theory which is widely used in molecular quantum chemistry, where it achieves high accuracy in the prediction of reaction energies for a wide range of systems. While being an efficient method for calculating small- to medium-sized molecules, single-reference CC methods have never been used to calculate the formation energies of silicon self-interstitials and the vacancy in diamond cubic crystal silicon. Only over the past few years have computationally efficient implementations of periodic CC methods become available to study such systems [37–40]. Moreover, recent developments in embedding approaches also make it possible to study such local phenomena using CC methods [41–49]. The goal of this work is to calculate the formation energies of the silicon self-interstitials and vacancy at the level of coupled cluster singles doubles and perturbative triples [CCSD(T)] theory and compare them to experimental data [8,27–29,33] and reference data from the literature [18,21,34,35].

## II. THEORY AND METHODS

### A. Hartree-Fock and CC theory

In Hartree-Fock (HF) theory, the many-body wave function is approximated by a single Slater determinant, and the energy is optimized with respect to variations of the spin orbitals used to construct the Slater determinant. The Slater determinant constructed from these spin orbitals is the HF ground state wave function  $|0\rangle$  and can be interpreted as a new vacuum from which particle-hole pair excitations are created and annihilated in the context of quantum field theory. Building on one-body theories such as HF, CC theory employs an exponential ansatz acting on a single Slater determinant.

$$|\Psi_{\text{CC}}\rangle = e^{\hat{T}}|0\rangle, \quad (1)$$

$$\hat{T} = \sum_{i,a} t_i^a \hat{a}_a^\dagger \hat{a}_i + \frac{1}{4} \sum_{i,j,a,b} t_{ij}^{ab} \hat{a}_a^\dagger \hat{a}_b^\dagger \hat{a}_j \hat{a}_i + \dots \quad (2)$$

Herein, the indices  $i, j$  and  $a, b$  refer to particle (unoccupied) and hole (occupied) states, respectively. By projecting onto the excited Slater determinants, one obtains a set of coupled nonlinear equations that can be solved for the amplitudes  $t_i^a$ ,  $t_{ij}^{ab}$ , etc., using iterative methods. For practical calculations, the cluster operator  $\hat{T}$  has to be truncated, usually to single and double excitations. While including the full triple excitation manifold is computationally too expensive, an estimate of the connected triples contribution can be calculated noniteratively using an expression reminiscent of many-body perturbation theory. This method is referred to as CCSD(T) theory [50]. A more detailed description of CC methods can be found in Refs. [51,52].

### B. Basis set and finite-size error correction

All practical post-Hartree-Fock calculations of real materials employ a finite number of particle states also referred to as virtual orbitals  $N_v$ . The truncation of the virtual orbital basis set introduces the basis set incompleteness error (BSIE). The BSIE vanishes very slowly in the limit of  $N_v \rightarrow \infty$ . This observation is not surprising since the leading order basis set error originates from the so-called electron-electron cusp conditions [53], which are, in real space, a short-range electronic correlation phenomenon. Explicitly correlated methods help reduce the finite basis set error substantially [54,55]. These methods, as well as their application to periodic systems, have already been discussed extensively elsewhere [56–58]. In order to treat the BSIE we use a pair-specific cusp correction for CC theory [59]. This scheme is based on frozen natural orbitals and diagrammatically decomposed contributions to the electronic correlation energy, which dominates the BSIE. To partly account for the BSIE of the T contribution to the CCSD(T) correlation energy, we rescale the T contribution using the ratio of the CCSD correlation energy with and without the BSIE correction discussed above.

Further, we simulate the silicon crystal using a periodic supercell approach with a finite system size. The employed finite system introduces the finite-size incompleteness error (FSIE). It should be noted that many properties, including the ground state energy, converge slowly with respect to the system size. This originates from the fact that correlated wave-function-based theories capture longer-range electronic correlation effects such as dispersion interaction explicitly. The coupled cluster correlation energy can be expressed as an integral over the electronic transition structure factor multiplied by the Coulomb kernel in reciprocal space. Finite-size errors partly originate from an incomplete sampling of this integral in reciprocal space. Here, we employ an interpolation technique that can be used to evaluate the correlation energy integral more accurately, reducing the finite-size error. The technical details are described in Ref. [60].

### C. Cell structure

The employed simulation cells of silicon self-interstitials are obtained by adding one Si atom to the diamond cubic crystal structure of bulk silicon and relaxing the atomic positions. The energetically most stable silicon self-interstitial (X) is one in which two silicon atoms reside symmetrically shifted from the position previously occupied by one. The two atoms are oriented parallel to the [110] direction. The second most favorable self-interstitial (H) is where the additional Si atom is equidistant to six other atoms, forming a hexagonal ring. It is worth noting that this configuration is unstable in DFT with the Perdew-Burke-Ernzerhof (PBE) functional, where the central atom of the ring is slightly moving away in a direction orthogonal to the ring (C3V) [18,61]. The last self-interstitial considered in this work, with the highest energy, is where the additional Si atom is coordinated equidistantly to four nearest neighbors, forming a tetrahedron (T). For the T interstitial, the highest occupied state is threefold degenerate but occupied by only two electrons, which potentially introduces a multireference character. The vacancy is created by removing one Si atom from the bulk structure. Like the

T interstitial, it has a threefold degenerate highest occupied state, occupied by two electrons. The vacancy is known to undergo a Jahn-Teller distortion to  $D_{2d}$  symmetry [62].

All the ion positions of the used structures have been relaxed at the DFT level using the PBE exchange and correlation energy functional [63]. The shape and volume of the cells are kept fixed during the relaxation procedure. The relaxed cells can be found in the POSCAR files in the GitHub/Zenodo repository [64,65].

#### D. Computational details

All coupled cluster calculations are performed using our high-performance open-source coupled cluster simulation code, Coupled Cluster for Solids (CC4S). The preparation of the necessary reference wave function and the required intermediates is performed using the Vienna Ab initio Simulation Package (VASP) [66–68]. For all calculations in VASP a plane-wave kinetic energy cutoff of  $E_{\text{cut}} = 400$  eV is used. The employed smearing parameter is  $\sigma = 10^{-4}$  eV, and a convergence criterion of  $\Delta E = 10^{-6}$  eV is used. All other numerical parameters are left unchanged from their default values. The HF calculations are performed using VASP and the structures described in Sec. II C. The HF calculations are done using a  $\Gamma$ -centered  $7 \times 7 \times 7$   $k$ -point mesh. All post-HF calculations sample the first Brillouin zone using only a single  $k$  point. Further, we need to write out all unoccupied HF orbitals since in CC theory we approximate the many-electron wave function using excited Slater determinants, constructed of occupied and unoccupied HF orbitals. In VASP this is achieved by setting the number of virtual orbitals to be written out (through the NBANDS flag) to the maximum number of plane waves in the basis set, which is specified by the energy cut of  $E_{\text{cut}}$ . The convergence of the coupled cluster singles doubles (CCSD) electron correlation energy is very slow when using canonical HF orbitals. A much faster convergence to the complete basis set limit is achieved using natural orbitals. In VASP approximate natural orbitals can be calculated as described in Eq. (2) in Ref. [69]. After calculating all natural orbitals, a subset of them is chosen for the CC4S calculations. For the coupled cluster theory calculations, we choose the number of unoccupied natural orbitals per occupied orbital to be 5, 10, 15, 20, 25, and 30. Additionally, for the basis set correction algorithm described in Sec. II B and in the references therein, the second-order Møller-Plesset perturbation theory (MP2) pair energies are needed. For this purpose, there are two algorithms available in VASP [70,71]. In our case, we use a 16-atom cell for the bulk with 32 occupied orbitals; therefore, the MP2 algorithm from Ref. [71] is more efficient. In the case of more than 50 occupied orbitals, a different algorithm based on Laplace transformed MP2 might be faster and less memory consuming [70]. Note that the basis set correction algorithm uses a focal-point approach, and from now on, the basis set correction is also referred to as the focal-point correction (FPC). With these preparations done, VASP can provide all necessary files needed for the CCSD(T) calculation with the finite-size and basis set error correction computed by CC4S. It is worth noting that the CCSD calculation in CC4S converges much faster when we use the direct inversion of the iterative subspace mixer instead of the default linear mixer.

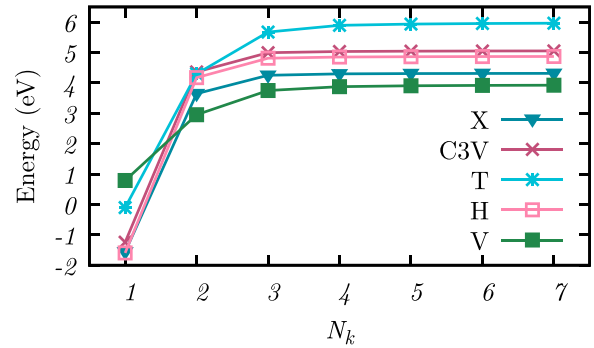


FIG. 1. The formation energy as a function of the number of  $k$  points used in the Hartree-Fock calculation for all self-interstitials. A  $\Gamma$ -centered cubic  $k$ -point mesh was used with  $N_k \times N_k \times N_k$  grid points.

The described workflow with all files necessary to reproduce the calculations can be found on GitHub or Zenodo [64,65].

After studying the BSIE, we chose our number of virtual orbitals per occupied orbital to be 10 and repeated all calculations with 10 randomly chosen  $k$ -point shifts in order to get a twist average estimate of the CCSD(T) correlation energies. The ratio of virtual orbitals to occupied orbitals is the same for all structures.

All calculations are performed using 16 compute nodes, each equipped with 384 GB main memory.

Further, we calculate the formation energies at the DFT level of theory, utilizing the Heyd–Scuseria–Ernzerhof (HSE) exchange correlation functional with up to  $5 \times 5 \times 5$   $k$  points (converged within 10–20 meV), as shown in Table II below.

### III. RESULTS

We now discuss the formation energies of the silicon self-interstitial structures described in Sec. II C at the CCSD(T) level of theory. We use 16 atom cells for the pristine bulk crystal with periodic boundary conditions; the interstitial cells have 17 atoms, while the vacancy has 15 atoms. The HF energies, CCSD, CCSD(T), and finite-size and basis set energy corrections can be found in Table I of the Supplemental Material [72]. The formation energy is calculated by subtracting the energy of the bulk cell from the energy of the interstitial cell scaled to the same number of atoms:

$$E_F = E_{\text{int}} - \frac{N_{\text{int}}}{N_{\text{bulk}}} E_{\text{bulk}}. \quad (3)$$

We first discuss the convergence of the HF energy contribution to the formation energies. Figure 1 shows the convergence of the HF formation energies with respect to the size of the  $k$ -point mesh used in the HF calculation. We used a  $\Gamma$ -centered cubic  $k$ -point mesh with up to  $7 \times 7 \times 7$  grid points. Using only one  $k$  point gives qualitatively and quantitatively wrong formation energies. With a  $k$ -point mesh size of  $5 \times 5 \times 5$ , the formation energies are already well converged, and increasing the  $k$ -point grid size further to  $7 \times 7 \times 7$  increases the formation energies of X, H, and C3V by less than 8.5 meV, while T and V increase by 29 and 19 meV. We now discuss the convergence of the correlation energy contributions to the formation energies with respect to the number of virtual or-

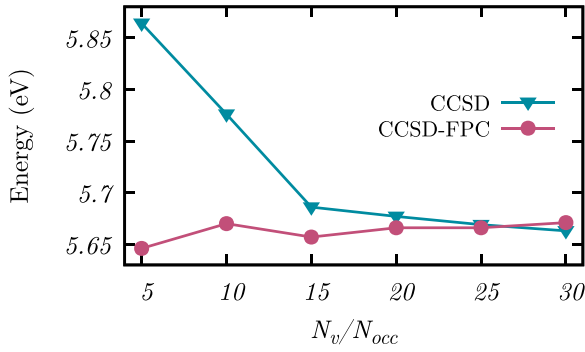


FIG. 2. CCSD formation energy of the X interstitial as a function of the number of orbitals per occupied orbital with and without the basis set correction scheme (FPC). A  $\Gamma$ -centered cubic mesh was used.

bitals. Let us note that the HF formation energy contributions are independent of the virtual orbital basis set size. The MP2 calculations employ the complete virtual orbital basis set defined by the kinetic energy cutoff of the plane wave basis set. Furthermore the MP2 correlation energies are automatically extrapolated to the complete basis set limit using a procedure explained in Ref. [70]. For the post-MP2 correlation energy calculations, we employ approximate natural orbitals as virtual orbitals and seek to converge the correlation energies explicitly by increasing the number of virtual orbitals. We find that this approach allows for an effective cancellation between basis set incompleteness errors of correlation energies for different systems when taking their differences. Furthermore, we add a basis set incompleteness error correction described in Ref. [59] to accelerate the convergence of the CCSD correlation energy. The effect of the basis set correction on the formation energy is highlighted in Fig. 2, which depicts the formation energy retrieved as a function of the number of virtual orbitals per occupied orbital for the X interstitial. Our results indicate that between 10 and 20 virtual orbitals per occupied orbital suffice to achieve converged formation energies with and without the basis set correction, respectively. The remaining basis set incompleteness error is caused by fluctuations on the scale of about 10 meV, which is smaller than the expected accuracy of the employed theories. Figure 3 shows the convergence of the CCSD(T) formation energies of all self-interstitials with respect to the number of natural orbitals, including the finite-size and basis set corrections. Note that the basis set correction behaves similarly for all self-interstitials. From Fig. 3, we see that  $N_v/N_{occ} = 10$  is already accurate enough to assume convergence within chemical accuracy ( $\approx 43$  meV).

With  $N_v/N_{occ} = 10$ , we repeat all calculations at 10 random  $k$  points in order to obtain a twist-averaged estimate of the correlation energy contribution to the formation energies. This approach reduces finite-size errors in CC calculations that originate from single-particle effects [39]. The energy corrections for the twist averaging can be found in Tables II–VII in the Supplemental Material. Using 10 random  $k$  points, our standard deviation from the average CCSD(T) energy is in decreasing order for  $E_F(T) = 227$  meV,  $E_F(V) = 101$  meV,  $E_F(X) = 80$  meV,  $E_F(C3V) = 73$  meV, and  $E_F(H) = 51$  meV. After twist averaging, the formation

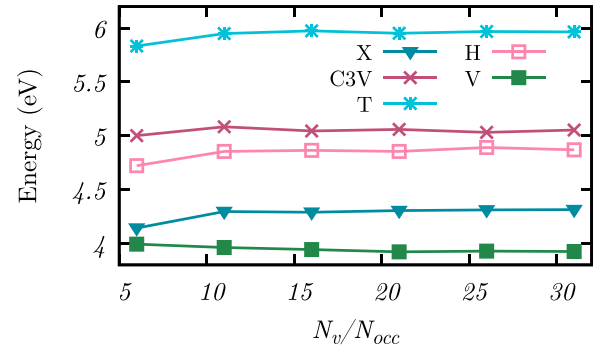


FIG. 3. CCSD(T) formation energies as a function of the number of virtual orbitals per occupied orbital for all self-interstitials include finite-size and basis set corrections.

energies of V, T, and X increase by 818, 367, and 239 meV. However, the formation energies of the C3V and H interstitials decrease by 85 and 44 meV, indicating that it is important to account for this contribution. The  $\Gamma$ -point formation energies are shown in Table I, while the twist-averaged formation energies are shown in Table II for X, H, and T and in Tables III and VII in the Supplemental Material for V and C3V.

Further, we calculate the formation energies at the DFT level of theory, utilizing the Heyd-Scuseria-Ernzerhof (HSE) exchange correlation functional again in Table I. The HF energies, CCSD, CCSD(T), and finite-size and basis set energy corrections can be found in Table I in the Supplemental Material.

Next, we briefly discuss the effect of the FSIE correction based on the structure factor interpolation, which accounts for two-electron finite-size errors. Table I summarizes the computed CCSD formation energies with and without the corresponding finite-size correction, denoted as CCSD-FS and CCSD, respectively. It is not surprising that this correction is significant and on the scale of about 0.5 eV. However, based on previous results reported in Ref. [39], we expect that the employed finite-size correction will suffice for the 16/17-atom cells to achieve chemical accuracy in the convergence of the computed formation energies with respect to the employed system size. Furthermore, it can be concluded from the comparison between CCSD-FS and CCSD in Table I that the computed finite-size correction is already well converged using  $N_v/N_{occ} = 10$ . Note that the finite-size correction can currently be applied only to the CCSD calculation. The T contribution to the formation energies is significantly smaller than the CCSD correlation energy contribution, which makes it plausible to neglect the finite-size correction to the T contribution. We emphasize that our finite-size correction scheme corrects for the incomplete sampling of the integral over the electronic transition structure factor, as described in Sec. II B. The finite-size error stemming from the interactions of the defects through the periodicity of the crystal remains and can be addressed only by increasing the cell size significantly, which is, for now, out of our computational reach.

Table I also includes results for the vacancy formation energy. We note that these calculations employ only a 15-atom cell. Due to the small supercell size, the system does not undergo a Jahn-Teller distortion [62], which can be observed

TABLE I. CCSD and CCSD(T) formation energies of the silicon self-interstitials and the vacancy with and without the basis set and finite-size corrections as a function of the unoccupied to occupied orbital ratio  $N_v/N_{occ}$  at the  $\Gamma$  point. FPC and FS denote that the basis set and finite-size corrections are included. All energies are in eV.

| HF/MP2 | $N_v/N_{occ}$ | CCSD  | CCSD(T) | CCSD-FS | CCSD-FPC | CCSD-FS-FPC | CCSD(T)-FS-FPC |
|--------|---------------|-------|---------|---------|----------|-------------|----------------|
| C3V    | 5             | 6.659 | 5.981   | 6.149   | 6.334    | 5.824       | 5.001          |
| 8.502  | 10            | 6.484 | 5.753   | 6.012   | 6.343    | 5.871       | 5.083          |
| 4.408  | 15            | 6.374 | 5.614   | 5.907   | 6.305    | 5.837       | 5.044          |
|        | 20            | 6.347 | 5.577   | 5.880   | 6.317    | 5.850       | 5.059          |
|        | 25            | 6.330 | 5.556   | 5.864   | 6.288    | 5.822       | 5.031          |
|        | 30            | 6.315 | 5.537   | 5.849   | 6.308    | 5.843       | 5.053          |
| X      | 5             | 5.864 | 5.094   | 5.285   | 5.646    | 5.067       | 4.142          |
| 7.930  | 10            | 5.776 | 4.982   | 5.254   | 5.670    | 5.148       | 4.296          |
| 3.780  | 15            | 5.686 | 4.866   | 5.169   | 5.657    | 5.141       | 4.289          |
|        | 20            | 5.677 | 4.853   | 5.162   | 5.666    | 5.150       | 4.305          |
|        | 25            | 5.669 | 4.842   | 5.155   | 5.666    | 5.152       | 4.311          |
|        | 30            | 5.663 | 4.831   | 5.150   | 5.671    | 5.158       | 4.313          |
| T      | 5             | 7.857 | 7.051   | 7.238   | 7.435    | 6.816       | 5.833          |
| 9.954  | 10            | 7.628 | 6.764   | 7.055   | 7.455    | 6.882       | 5.949          |
| 5.355  | 15            | 7.531 | 6.641   | 6.964   | 7.469    | 6.902       | 5.974          |
|        | 20            | 7.511 | 6.611   | 6.944   | 7.447    | 6.880       | 5.952          |
|        | 25            | 7.489 | 6.584   | 6.923   | 7.458    | 6.892       | 5.968          |
|        | 30            | 7.476 | 6.565   | 6.910   | 7.456    | 6.890       | 5.964          |
| H      | 5             | 6.358 | 5.717   | 5.877   | 5.986    | 5.504       | 4.722          |
| 8.162  | 10            | 6.231 | 5.538   | 5.783   | 6.053    | 5.605       | 4.854          |
| 4.212  | 15            | 6.132 | 5.413   | 5.689   | 6.058    | 5.615       | 4.864          |
|        | 20            | 6.103 | 5.376   | 5.661   | 6.046    | 5.604       | 4.854          |
|        | 25            | 6.090 | 5.360   | 5.649   | 6.075    | 5.635       | 4.890          |
|        | 30            | 6.075 | 5.341   | 5.634   | 6.056    | 5.616       | 4.869          |
| V      | 5             | 5.291 | 4.866   | 4.820   | 4.999    | 4.528       | 3.993          |
| 5.554  | 10            | 5.034 | 4.546   | 4.573   | 4.952    | 4.492       | 3.961          |
| 4.305  | 15            | 4.960 | 4.443   | 4.500   | 4.942    | 4.483       | 3.942          |
|        | 20            | 4.942 | 4.413   | 4.484   | 4.925    | 4.467       | 3.921          |
|        | 25            | 4.926 | 4.394   | 4.470   | 4.928    | 4.472       | 3.928          |
|        | 30            | 4.919 | 4.380   | 4.462   | 4.928    | 4.472       | 3.924          |

for larger cells and which significantly changes the formation energy. Therefore, we note that these results are meaningful only as benchmarks for other theories employing identical geometries and cannot be compared to experiment. Our best estimates of the formation energies at the level of HF, CCSD, and CCSD(T) including all corrections discussed above are compared to values from the literature and experiment in Table II. We see that the formation energies calculated with LDA and PBE are small (3–4 eV) and close to each other for all self-interstitials, with a difference of 80–160 meV. Yet the order of stability is not the same; for LDA the most stable self-interstitial is X, then H and T. For PBE T has a lower energy than H. Incorporating a portion of the exact exchange correlation energy in the HSE functional increases the formation energies and their differences to 200 meV between X and H and 70 meV between H and T with the order of stability of X, H, and T. The random-phase approximation (RPA) predicts the same order of stability with a difference between X and H of 180 meV, while the difference between H and T is 80 meV. Increasing the cell size to 216 atoms changes the differences significantly to 130 and 600 meV, still with the same order of stability. Note that the 16-atom cell structures used for the RPA and PBE calculations from Ref. [35] are

identical to ours.  $G_0W_0$  for 16-atom cells predicts that H is more stable than X, while their difference is only 60 meV. In QMC, using 16-atom cells without a backflow correction, X and H are nearly degenerate, while the difference from T is 300 meV. Including the backflow correction gives the order of stability as X, H, and T with clear differences of 300 and 400 meV. We now turn to the wave function methods employed in this work. The formation energies calculated with HF are much larger than the ones calculated with the other theories presented. While the order of stability is in agreement with the corrected QMC calculations, their difference is 232 and 1792 meV. Expanding the correlation space further to CCSD and CCSD(T) theory, including the basis set and finite-size correction, lowers the formation energies by 2.8–2.6 eV and another 811–749 meV. Their relative difference also changes to 264 and 1568 meV for CCSD theory and 275 and 1506 meV for CCSD(T) theory. Our estimated CCSD(T) formation energies are in good agreement with extrapolated QMC calculations [34] employing a Slater-Jastrow-backflow correction for the X and H interstitials. However, we have a discrepancy of 1.2 eV for the T interstitial. This could stem from the fact that in DFT the energetically highest occupied orbitals are threefold degenerate while being occupied by

TABLE II. Computed and converged HF, CCSD, CCSD(T), and HSE formation energies, including all reported corrections in this work compared to QMC [34], RPA [35], PBE [35], LDA [18,21], and  $G_0W_0$  [18] from the literature and also experimental data [8,27–29,33]. All results have been obtained for the 16/17-atom cells except RPA (216), which employed 216/217-atom cells.

| Cell | HF    | CCSD  | CCSD(T) | QMC | QMC (nobf) | $G_0W_0$ | RPA  | RPA (216) | HSE  | PBE  | LDA  | Expt.   |
|------|-------|-------|---------|-----|------------|----------|------|-----------|------|------|------|---------|
| X    | 7.930 | 5.295 | 4.535   | 4.4 | 4.9        | 4.46     | 4.27 | 4.2       | 4.17 | 3.56 | 3.29 |         |
| T    | 9.954 | 7.127 | 6.316   | 5.1 | 5.2        |          | 4.53 | 4.93      | 4.44 | 3.66 | 3.56 |         |
| H    | 8.162 | 5.559 | 4.810   | 4.7 | 4.9        | 4.4      | 4.45 | 4.33      | 4.37 | 3.74 | 3.4  | 4.2–4.7 |

two electrons. It may be an indication that a multireference treatment is needed. Our CCSD(T) formation energy for the H interstitial is within reasonable agreement with experiment, being 110 meV above the experimental upper bound.

#### IV. CONCLUSION AND SUMMARY

In this paper, we calculated the formation energies of the silicon self-interstitials and the vacancy in a periodic supercell at the CCSD(T) level of theory. We used correction schemes tailored to CC theory to reduce the BSIE and the FSIE. Our results were compared to data from the literature and experiment, including LDA, PBE, HSE, RPA,  $G_0W_0$ , and QMC.

In general, DFT using the LDA and PBE functionals fails to differentiate the structures, resulting in small energy differences between the self-interstitials while also underestimating the formation energies. Additionally, HF overestimates the formation energies. The HSE functional offers a compromise, and its formation energies are in good agreement with the much more expensive and accurate QMC calculations. The QMC formation energies of the two most stable self-interstitials, X and H, are nearly degenerate. This degeneracy is lifted by employing the Slater-Jastrow-backflow trial wave function [34].

Our CCSD(T) formation energies are in good agreement with QMC calculations employing a Slater-Jastrow-backflow wave function for the X and H interstitials. The CCSD(T) formation energy for the H interstitial is within reasonable agreement with experimental data, being 110 meV above the upper bound. However, the CCSD(T) formation energy of the T interstitial is 1.2 eV higher than in the QMC calculations. Since in DFT the highest occupied orbital of the T interstitial

is threefold degenerate but occupied by only two electrons, we suppose a multireference approach may be necessary. We stress that none of the discussed methods is expected to work for strongly correlated systems. DFT-based approaches underestimate the formation energy of strongly correlated defects due to the introduction of partly filled orbitals that reduce the self-interaction error. QMC techniques require multiterminant trial wave functions for strongly correlated systems to reduce the error from the fixed-node approximations, and RPA is expected to inherit some of the DFT errors for the treatment of strongly correlated systems. Therefore, we have to conclude that more sophisticated theories will be needed in future studies to fully resolve the observed discrepancy for the formation energy of the T interstitial.

Although we demonstrated that basis set convergence can be achieved efficiently at the level of CCSD(T) theory using recently presented methods, the treatment of finite-size errors is still challenging, and relatively large defect concentrations had to be employed. However, we note that recently developed embedding methods will allow us to investigate much lower defect concentrations in a computationally efficient manner [48].

#### ACKNOWLEDGMENTS

The authors gratefully acknowledge support and funding from the European Research Council (ERC) under the European Union's Horizon 2020 research and innovation program (Grant Agreement No. 715594). The computational results presented were achieved using the Vienna Scientific Cluster (VSC).

- [1] K. Graff, *Metal Impurities in Silicon-Device Fabrication*, Springer Series in Materials Science, Vol. 24 (Springer, Berlin, Heidelberg, 2000).
- [2] E. Weber, *Krist. Tech.* **16**, 209 (1981).
- [3] S. T. Pantelides, *Deep Centers in Semiconductors a State-Of-The-Art Approach*, 2nd ed. (Gordon and Breach Science Publishers, Yverdon, Switzerland, 1992).
- [4] G. D. Watkins, *Mater. Sci. Semicond. Process.* **3**, 227 (2000).
- [5] O. Breitenstein and J. Heydenreich, *Scanning* **7**, 273 (1985).
- [6] N. Fukata and M. Suezawa, *J. Appl. Phys.* **86**, 1848 (1999).
- [7] R. J. Tilley, in *Encyclopedia of Inorganic and Bioinorganic Chemistry* (Wiley, Hoboken, NJ, 2018), pp. 1–23.
- [8] P. M. Fahey, P. B. Griffin, and J. D. Plummer, *Rev. Mod. Phys.* **61**, 289 (1989).
- [9] D. J. Eaglesham, P. A. Stolk, H. Gossmann, and J. M. Poate, *Appl. Phys. Lett.* **65**, 2305 (1994).
- [10] D. A. Richie, J. Kim, S. A. Barr, K. R. A. Hazzard, R. Hennig, and J. W. Wilkins, *Phys. Rev. Lett.* **92**, 045501 (2004).
- [11] R. Vaidyanathan, M. Y. L. Jung, and E. G. Seebauer, *Phys. Rev. B* **75**, 195209 (2007).
- [12] D. Riedel, F. Fuchs, H. Kraus, S. Vāth, A. Sperlich, V. Dyakonov, A. A. Soltamova, P. G. Baranov, V. A. Ilyin, and G. V. Astakhov, *Phys. Rev. Lett.* **109**, 226402 (2012).
- [13] A. M. Tyryshkin, S. Tojo, J. J. L. Morton, H. Riemann, N. V. Abrosimov, P. Becker, H.-J. Pohl, T. Schenkel, M. L. W. Thewalt, K. M. Itoh, and S. A. Lyon, *Nat. Mater.* **11**, 143 (2012).
- [14] K. Otsuka and X. Ren, *Intermetallics* **7**, 511 (1999).
- [15] W. Gao and A. Tkatchenko, *Phys. Rev. Lett.* **111**, 045501 (2013).
- [16] F. Bruneval, *Phys. Rev. Lett.* **108**, 256403 (2012).
- [17] R. Ramprasad, H. Zhu, P. Rinke, and M. Scheffler, *Phys. Rev. Lett.* **108**, 066404 (2012).

- [18] P. Rinke, A. Janotti, M. Scheffler, and C. G. Van de Walle, *Phys. Rev. Lett.* **102**, 026402 (2009).
- [19] C. G. Van de Walle and A. Janotti, *Phys. Status Solidi B* **248**, 19 (2011).
- [20] C. G. Van de Walle and J. Neugebauer, *J. Appl. Phys.* **95**, 3851 (2004).
- [21] E. R. Batista, J. Heyd, R. G. Hennig, B. P. Uberuaga, R. L. Martin, G. E. Scuseria, C. J. Umrigar, and J. W. Wilkins, *Phys. Rev. B* **74**, 121102(R) (2006).
- [22] W.-K. Leung, R. J. Needs, G. Rajagopal, S. Itoh, and S. Ihara, *Phys. Rev. Lett.* **83**, 2351 (1999).
- [23] P. E. Blöchl, E. Smargiassi, R. Car, D. B. Laks, W. Andreoni, and S. T. Pantelides, *Phys. Rev. Lett.* **70**, 2435 (1993).
- [24] Y. Bar-Yam and J. D. Joannopoulos, *Phys. Rev. B* **30**, 1844 (1984).
- [25] V. Ranki and K. Saarinen, *Phys. Rev. Lett.* **93**, 255502 (2004).
- [26] H. Bracht, J. F. Pedersen, N. Zangenberg, A. N. Larsen, E. E. Haller, G. Lulli, and M. Posselt, *Phys. Rev. Lett.* **91**, 245502 (2003).
- [27] A. Ural, P. B. Griffin, and J. D. Plummer, *Phys. Rev. Lett.* **83**, 3454 (1999).
- [28] H. Bracht, E. E. Haller, and R. Clark-Phelps, *Phys. Rev. Lett.* **81**, 393 (1998).
- [29] H. Bracht, N. A. Stolwijk, and H. Mehrer, *Phys. Rev. B* **52**, 16542 (1995).
- [30] H. Bracht, H. H. Silvestri, I. D. Sharp, and E. E. Haller, *Phys. Rev. B* **75**, 035211 (2007).
- [31] Y. Shimizu, M. Uematsu, and K. M. Itoh, *Phys. Rev. Lett.* **98**, 095901 (2007).
- [32] S. Dannefaer, P. Mascher, and D. Kerr, *Phys. Rev. Lett.* **56**, 2195 (1986).
- [33] A. Ural, P. B. Griffin, and J. D. Plummer, *J. Appl. Phys.* **85**, 6440 (1999).
- [34] W. D. Parker, J. W. Wilkins, and R. G. Hennig, *Phys. Status Solidi B* **248**, 267 (2011).
- [35] M. Kaltak, J. Klimeš, and G. Kresse, *Phys. Rev. B* **90**, 054115 (2014).
- [36] W. K. Leung, R. Needs, G. Rajagopal, S. Itoh, and S. Ihara, *VLSI Design* **13**, 229 (2001).
- [37] G. H. Booth, A. Grüneis, G. Kresse, and A. Alavi, *Nature (London)* **493**, 365 (2013).
- [38] T. Gruber and A. Grüneis, *Phys. Rev. B* **98**, 134108 (2018).
- [39] T. Gruber, K. Liao, T. Tsatsoulis, F. Hummel, and A. Grüneis, *Phys. Rev. X* **8**, 021043 (2018).
- [40] J. McClain, Q. Sun, G. K.-L. Chan, and T. C. Berkelbach, *J. Chem. Theory Comput.* **13**, 1209 (2017).
- [41] M. Schütz, L. Maschio, A. J. Karttunen, and D. Usvyat, *J. Phys. Chem. Lett.* **8**, 1290 (2017).
- [42] D. Usvyat, L. Maschio, and M. Schütz, *Wiley Interdiscip. Rev.: Comput. Mol. Sci.* **8**, 1 (2018).
- [43] M. Nusspickel and G. H. Booth, *Phys. Rev. X* **12**, 011046 (2022).
- [44] J. Chen, N. A. Bogdanov, D. Usvyat, W. Fang, A. Michaelides, and A. Alavi, *J. Chem. Phys.* **153**, 204704 (2020).
- [45] J. Sauer, *Acc. Chem. Res.* **52**, 3502 (2019).
- [46] H. H. Lin, L. Maschio, D. Kats, D. Usvyat, and T. Heine, *J. Chem. Theory Comput.* **16**, 7100 (2020).
- [47] J. D. Goodpaster, T. A. Barnes, F. R. Manby, and T. F. Miller, *J. Chem. Phys.* **140**, 18A507 (2014).
- [48] T. Schäfer, F. Libisch, G. Kresse, and A. Grüneis, *J. Chem. Phys.* **154**, 011101 (2021).
- [49] B. T. G. Lau, G. Knizia, and T. C. Berkelbach, *J. Phys. Chem. Lett.* **12**, 1104 (2021).
- [50] K. Raghavachari, G. W. Trucks, J. A. Pople, and M. Head-Gordon, *Chem. Phys. Lett.* **157**, 479 (1989).
- [51] R. J. Bartlett and M. Musiał, *Rev. Mod. Phys.* **79**, 291 (2007).
- [52] R. J. B. Isaiah Shavitt, *Many-Body Methods in Chemistry and Physics MBPT and Coupled-Cluster Theory*, Cambridge Molecular Science (Cambridge University Press, Cambridge, 2009).
- [53] T. Kato, *Commun. Pure Appl. Math.* **10**, 151 (1957).
- [54] C. Hättig, W. Klopper, A. Köhn, and D. P. Tew, *Chem. Rev.* **112**, 4 (2012).
- [55] S. Ten-no, *Theor. Chem. Acc.* **131**, 1070 (2012).
- [56] A. Grüneis, *Phys. Rev. Lett.* **115**, 066402 (2015).
- [57] A. Grüneis, J. J. Shepherd, A. Alavi, D. P. Tew, and G. H. Booth, *J. Chem. Phys.* **139**, 084112 (2013).
- [58] D. Usvyat, *J. Chem. Phys.* **139**, 194101 (2013).
- [59] A. Irmeler, A. Gallo, and A. Grüneis, *J. Chem. Phys.* **154**, 234103 (2021).
- [60] K. Liao and A. Grüneis, *J. Chem. Phys.* **145**, 141102 (2016).
- [61] O. K. Al-Mushadani and R. J. Needs, *Phys. Rev. B* **68**, 235205 (2003).
- [62] F. Corsetti and A. A. Mostofi, *Phys. Rev. B* **84**, 035209 (2011).
- [63] J. P. Perdew, K. Burke, and M. Ernzerhof, *Phys. Rev. Lett.* **77**, 3865 (1996).
- [64] F. Salihbegovic, <https://github.com/salihbegovic/Silicon-CCSD-T->.
- [65] F. Salihbegovic, <https://doi.org/10.5281/zenodo.8059574>.
- [66] G. Kresse and J. Hafner, *Phys. Rev. B* **47**, 558 (1993).
- [67] G. Kresse and J. Furthmüller, *Phys. Rev. B* **54**, 11169 (1996).
- [68] G. Kresse and J. Furthmüller, *Comput. Mater. Sci.* **6**, 15 (1996).
- [69] A. Grüneis, G. H. Booth, M. Marsman, J. Spencer, A. Alavi, and G. Kresse, *J. Chem. Theory Comput.* **7**, 2780 (2011).
- [70] T. Schäfer, B. Ramberger, and G. Kresse, *J. Chem. Phys.* **146**, 104101 (2017).
- [71] M. Marsman, A. Grüneis, J. Paier, and G. Kresse, *J. Chem. Phys.* **130**, 184103 (2009).
- [72] See Supplemental Material at <http://link.aps.org/supplemental/10.1103/PhysRevB.108.115125> for the raw data used to calculate the formation energies.